Facile Synthesis of Viral Templated Photocatalysts for Environmental Applications

Doreen Burchell
Senior Honors Thesis Tufts University, 4/19/2011

Abstract

As petroleum based fuels are becoming more difficult to locate and extract, alternate sources of energy as well as more efficient methods for their extraction require immediate attention. Water splitting is a promising alternative for the production of hydrogen fuel from light and water. Titanium dioxide is a common, non-toxic and inexpensive photoactive material capable of catalyzing this reaction. In this experiment, genetically modified tobacco mosaic virus assembled on functionalized glass served as a template for the formation of nanoscale titanium dioxide particles through an adsorption-hydrolysis cycle reaction of titanium dioxide precursors. Characterization of the surface composition of the material through XPS showed the material consisted of majority titanium dioxide and some titanium trioxide with oxygen and titanium in a 2:1 ratio. Examination of surface morphology through AFM revealed particle sizes increased with increasing cycle number. Tunable virus surface assembly density and particle size offer two dimensions of control with which the photocatalytically active titanium dioxide is synthesized in the pursuit toward fabrication of more efficient catalytic materials.

Table of Contents

1. Introduction **1**

1.1 Motivation and Goals 1
1.2 Background 2

2. Methods **4**

2.1 Instrumentation 4
2.2 TMV Surface Assembly 5
2.3 Platinum Loading 6
2.4 Activity Characterization 6

3. Results and Discussion **7**

3.1 Substrate Comparison 7
3.2 Titanium Dioxide Loading 10
3.3 Platinum Loading 13
3.4 Surface Characterization 14
3.5 Activity Characterization 27

4. Conclusions **32**
5. Appendix **34**
6. Works Cited **37**

1. Introduction

1.1 Motivation and Goals

As petroleum based fuels are becoming more difficult to locate and extract, alternate sources of energy as well as more efficient methods for their extraction require immediate attention. Water splitting is a promising alternative for the production of hydrogen fuel from light and water. Titanium dioxide is a common, non-toxic and inexpensive photoactive material capable of catalyzing this reaction. In this experiment, genetically modified tobacco mosaic virus assembled on functionalized glass served as a template for the formation of nanoscale titanium dioxide particles through an adsorption-hydrolysis cycle reaction of titanium dioxide precursors. A simple technique to fabricate nanoscale titanium dioxide particles for a water splitting reaction executed under mild conditions using a viral template is proposed.

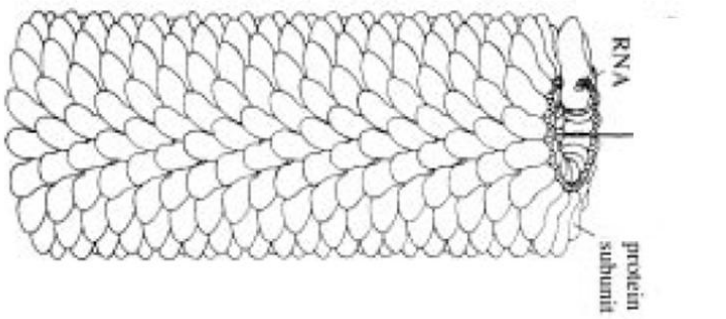

[1]

Figure 1: Representation of tobacco mosaic virus

The goal of this experiment is to easily and reproducibly fabricate controllable, nanoscale and photocatalytically active metal oxide for water-splitting. Specifically, the target was to form titanium dioxide nanoparticles on genetically modified tobacco mosaic virus (TMV 1-cys). As shown in Figure 1,

[1] A. Klug. The tobacco mosaic virus particle: structure and assembly. Philosophical Transactions Royal Society London B Biological Sciences. 1999 March 29; 354(1383): 531–535

TMV 1-cys is cylindrical in shape, 300nm long and 18nm in diameter with a 4nm open inner channel[2]. The genetically modified virus expresses coat proteins containing regularly spaced cysteine residues at the one position. The –SH groups on each cysteine is capable of forming strong metal-thiol bonds utilized in previous works as nucleation sites for noble metal particle growth.[3]

1.2 Background

Photocatalytic water splitting reactions are possible when the conduction band of the catalyst is higher (more negative) than the energy level of hydrogen formation from water and the valence band energy level is lower (less negative) than the energy level for oxygen formation from water. The process is represented in Figure 2. Upon activation by ultra-violet light, titanium dioxide excites electrons from their valance band energy state to its conductance band, thereby creating electron and electron hole pairs, capable of driving unfavorable reactions to detectable yields. The excitation of an electron in titanium dioxide is shown in Equation 3.

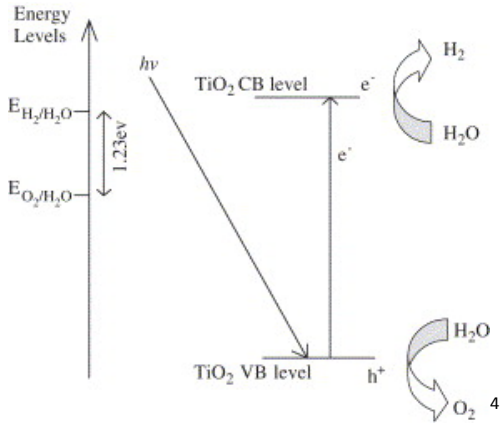

Figure 2: Energy Band Diagram for the water splitting reaction catalyzed by TiO_2.

[2] Cuixian Yang , Amy K. Manocchi , Byeongdu Lee , Hyunmin Yi a,. *Viral templated palladium nanocatalysts for dichromate reduction*. Applied Catalysis B: Environmental (2010) Volume 93, Issues 3-4,Jan. 12, Pages 282-291

[3] Ibid.

[4] Meng Ni, Michael K.H. Leung, Dennis Y.C. Leung, K. Sumathy, A review and recent developments in photocatalytic water-splitting using TiO2 for hydrogen production, Renewable and Sustainable Energy Reviews, Volume 11, Issue 3, April 2007, Pages 401-425.

The typical method for fabricating titanium dioxide particles utilizes a titanium dioxide precursor solution which is reduced or hydrolyzed in order to form solid titanium dioxide. Previous experiments utilized titanium (IV) bis(ammonium lactatato)dihydroxide (TALH), titanium (IV) isopropoxide and titanium (IV) butoxide precursors whose structures are shown in Figure 3. These precursors undergo the reactions described in Equation 1 and Equation 2 to form titanium dioxide[5].

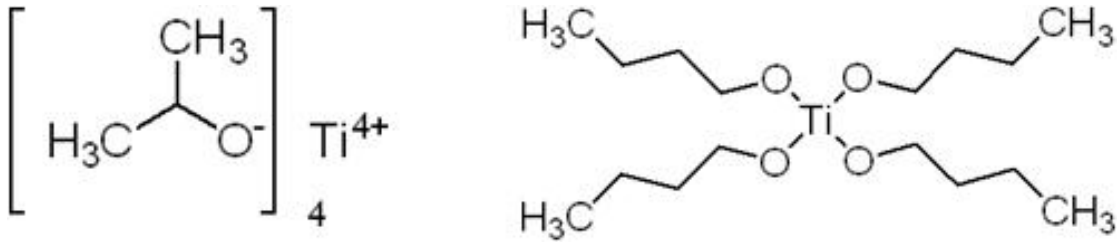

Figure 3: Titanium (IV) isopropoxide and titanium (IV) butoxide

$$\boldsymbol{Ti(OC_4H_9)_4 + 4H_2O \rightarrow Ti(OH)_4 + 4C_4H_9OH} \qquad \textbf{Equation 1}$$

$$\boldsymbol{Ti(OH)_4 \rightarrow TiO_2 + 2H_2O} \qquad \textbf{Equation 2}$$

In this experiment, the properties of the TMV-1-cys bio-template will be used to exercise two dimensions of control over the size and number of particles formed. By tuning the surface coverage density of the substrate, the number of particles capable of forming can be controlled. The size of the particle can then be controlled by the number of repetitions of the adsorption-hydrolysis reactions executed. This experiment will measure, characterize and test the activity of the material formed through these methods in the pursuit of a more efficient photocatalyst.

[5] Takayuki Hirai, Hiroshi Sato, Isao Komasawa. Mechanism of formation of titanium dioxide ultrafine particles in reverse micelles by hydrolysis of titanium tetrabutoxide. T*Industrial & Engineering Chemistry Research* **1993** *32* (12), 3014-3019

[6]

Equation 3: Electron excitation in titanium dioxide

2. **Methods**

2.1 Instrumentation

The Atomic Force Microscope (AFM) was the primary tool used in obtaining visual data about the morphology and topology of the virus and metal oxide particles. Using a delicate cantilever, the machine vibrates the cantilever tip at its resonant frequency, using a laser to detect deflections caused by the topology of the sample in order to measure the heights throughout a representative area of the sample and form an accurate, nanoscale topographical map. A Veeco Dimension V 3100 Atomic Force Microscope was used to image the samples as well as observe and quantify differences in heights and roughness of the TMV 1-cys rods after each material deposition procedure.

X-ray photoelectron spectroscopy (XPS) was used to characterize the surface chemistry of the fabricated samples. XPS analysis involves irradiating a sample with X-rays and measuring the energy and number of electrons emitted by the sample. This data yields a plot of the number of electrons detected per unit time (counts per second: CPS) versus their binding energy in electron volts (eV). When the element is irradiated, peaks of high count rate will be detected at its characteristic binding energy and the element and its current oxidation state can be uniquely identified.

[6] Meng Ni, Michael K.H. Leung, Dennis Y.C. Leung, K. Sumathy, *A review and recent developments in photocatalytic water-splitting using TiO2 for hydrogen production* Renewable and Sustainable Energy Reviews Volume 11, 2007, Pages 401–425.

$$2\,H_2O \rightarrow O_2 + 4\,H^+ + 4\,e^-$$
$$4\,H^+ + 4\,e^- \rightarrow 2\,H_2$$

Equation 4: Water splitting reaction

2.2 TMV Assembly

The various substrates used throughout this experiment were incubated in a solution of 0.1mg/mL TMV-1-cys solution overnight. The chips were then rinsed with deionized water and dried with inert nitrogen gas. One cycle of hydrolysis reactions of titanium dioxide precursors were performed by immersing the chip in 100mM precursor solution for one minute, rinsing the chip with the precursor solvent and immersing the chip in water for one minute. This procedure was repeated to achieve higher cycle numbers. Substrates included gold, glass slides and glass slides functionalized with aldehyde groups or epoxy groups. Titanium (IV) butoxide and titanium (IV) isopropoxide precursors were used in the hydrolysis reactions in ethanol and toluene-ethanol solvents respectively. A schematic of the procedure

Precursor	**Concentration (M)**	**Solvent**
Titanium (IV) isopropoxide (TIPP)	0.1	Ethanol (>99%)
Titanium (IV) butoxide (TiBu)	0.1	1:1 toluene: ethanol mixture

is shown in

Figure 4.

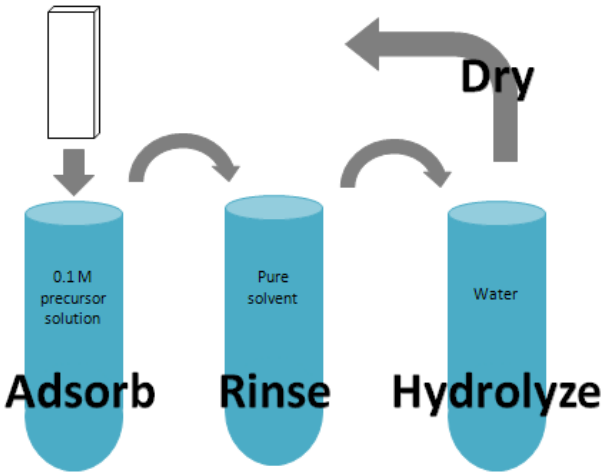

Precursor	Concentration (M)	Solvent
Titanium (IV) isopropoxide (TIPP)	0.1	Ethanol (>99%)
Titanium (IV) butoxide (TiBu)	0.1	1:1 toluene: ethanol mixture

Figure 4: Schematic representation 1 cycle of the hydrolysis reaction procedure

2.3 Platinum Loading

During the course of this experiment, a number of TMV chips were loaded with platinum through the reduction of a platinum precursor with a sodium borohydride reducing agent. To load the TMV template chip with platinum, the TMV assembled chip was dipped in a solution containing 5mM platinum precursor, Na_2PtCl_6 and a 0.5mM reducing agent of $NaBH_4$ was added and allowed to react for 20 min. The samples were then rinsed with dionized water and dried with nitrogen gas.

2.4 Activity Characterization

The potential photocatalytic activity of the chips fabricated in the preceding stages of this experiment was examined using the setup photographed and schematically represented in Figure 5. A UV chamber (Electro-Lite ELC 500) was used to expose chips of about a $1cm^2$ area immersed in 25mL of deionized water within a quartz flask. A dissolved oxygen (DO) probe (Orion) was used to measure the amount of dissolved oxygen in water. The amount of hydrogen evolved is then calculated stoichiometrically under

the assumption that the reactions occurs according to Equation 4. Water in the flask was flushed with nitrogen gas and stirred at the same rate for each experiment.

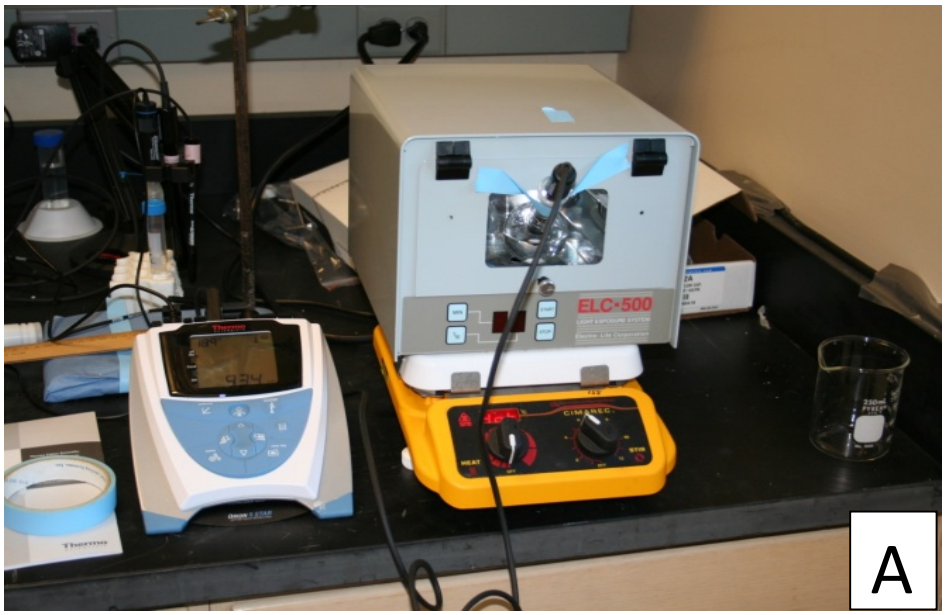

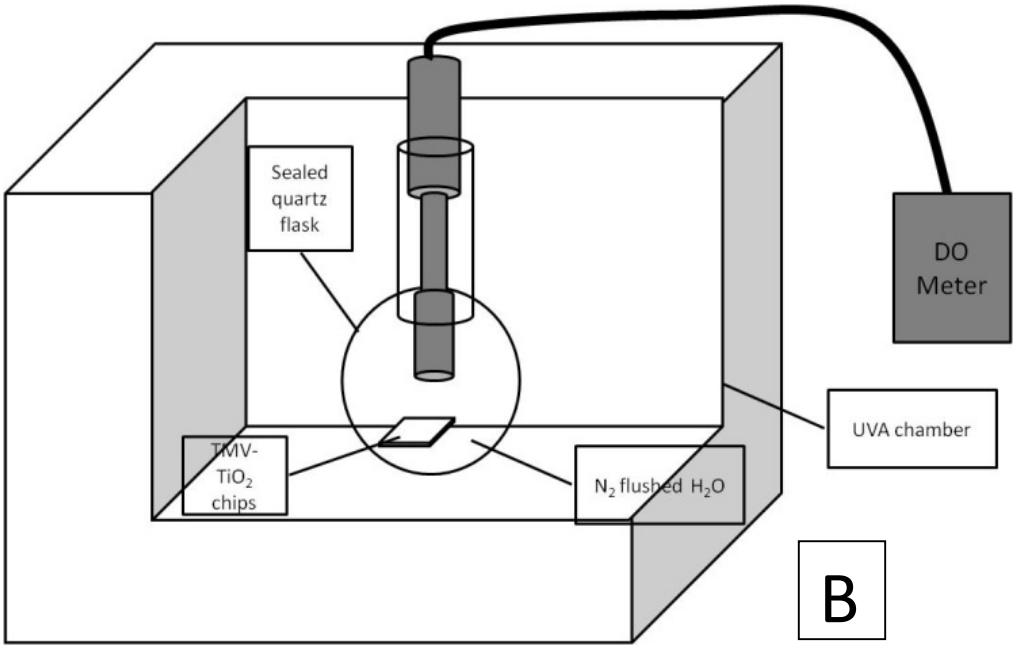

Figure 5: (A) Image and (B) schematic representation of the reactor setup.

3. Results and Discussion

3.1 Substrate Comparison

TMV 1-cys was assembled on a solid substrate for the target liquid phase water-splitting surface reaction. Gold chip substrates effectively achieved high TMV 1-cys coverage densities. The density of the TMV coverage was easily controlled through the concentration of the TMV solution in which the substrate was incubated. As shown in Figure 6, TMV solutions of greater concentration achieved higher surface coverage densities than those of lower concentrations.

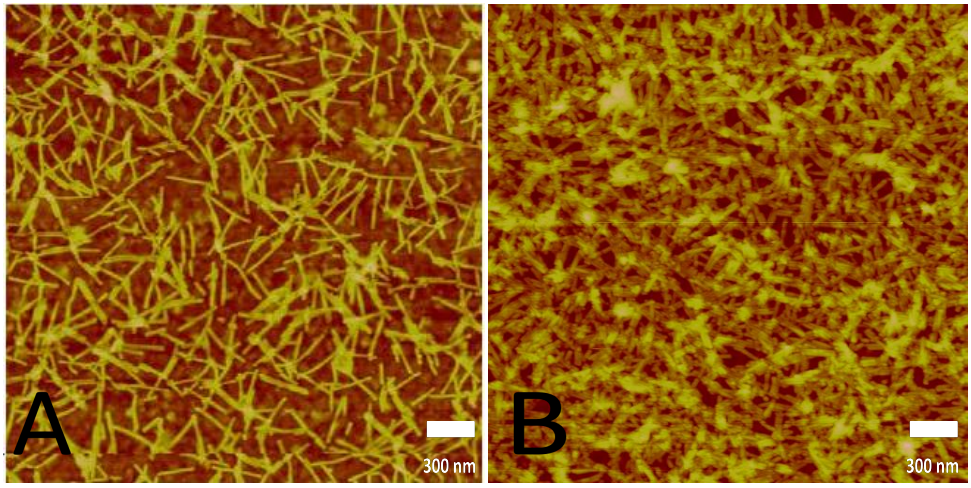

Figure 6: AFM images of gold substrates assembled with TMV from (A) 0.1mg/mL and (B) 0.25mg/mL

A cheaper and more practical substrate was sought out in the use of glass microscope slides treated with sodium hydroxide in order to increase the slide's surface hydrophilicity and achieve a stronger bond with the TMV 1-cys rods than would untreated glass. The slide becomes more hydrophilic after the NaOH treatment because the strong base is able to clean and etch the surface of glass and create more polar, almost negatively charged -OH groups. The increased hydrophilicity was observed visually when

water droplets flattened out over the surface of the glass instead of beading as it did on the untreated slides. Low and Non-uniform surface coverage densities of the virus were obtained using this hydrophilic glass substrate shown in Figure 8 D. The polar interactions between the glass surface groups and functional groups of TMV coat proteins did not appear to be strong enough to cause the high surface coverage density required for the intended application of the fabricated chips.

The coverage density increased, however with the use of functionalized glass slides which contain reactive functional groups on its surface. Epoxy functionalized slides were expected to achieve high densities because of the reactive ring shown in Figure 7 A. Due to the small three-atom ring, the group is highly strained easily opened through a substitution reaction to bond almost indiscriminately. The cysteine residues on the TMV as well as any other functional groups in the coat protein of the virus are available to react with the ring and covalently bond to ideally achieve high density, robust binding of the virus and substrate. As shown in Figure 8, this did not occur. Epoxy functionalized glass achieved low density and nonuniform TMV-1cys binding unusable for the intended purposes of the catalyst.

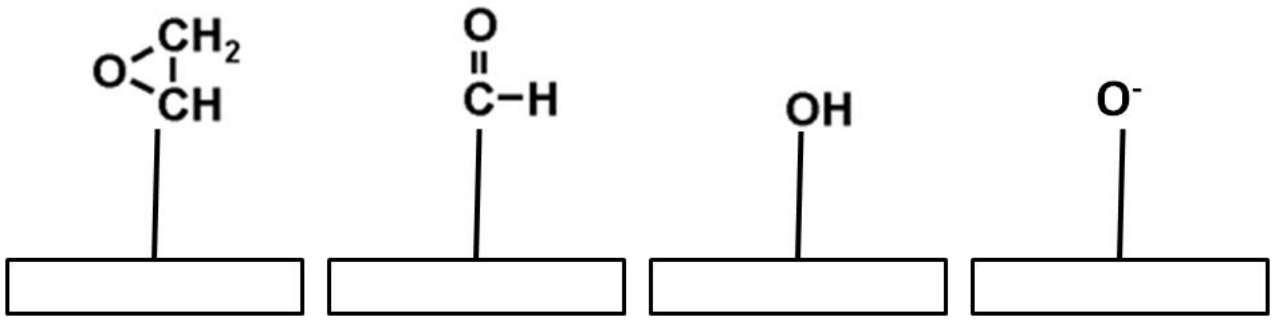

Figure 7: (A) Expoy functionalized (B) Aldehyde functionalized (C) Clean (D) NaOH treated glass slides.

Aldehyde functionalized glass achieved the highest and most uniform surface coverage density after incubation in 0.1mg/mL TMV solution. Figure 8 C shows an AFM image of a typical TMV assembled aldehyde glass slide. This density could similarly be increased or decreased with the concentration of the

TMV solution on aldehyde functionalized glass as on gold substrates. It was expected that aldehyde functionalized glass would form uniform and dense TMV coverage because the aldehyde group can react strongly with the polar functional groups of the TMV coat proteins including cysteine to form covalent bonds between the virus and glass surface.

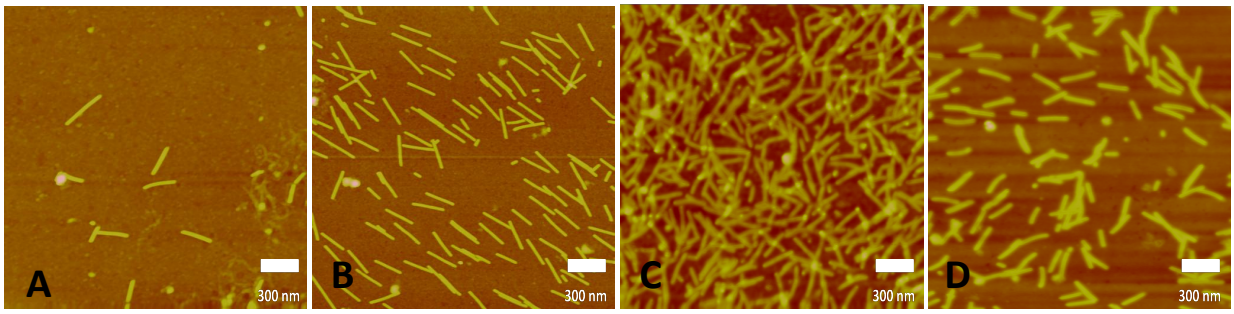

Figure 8: 3µm x 3 µm AFM images of TMV 1-cys assembled on (A) epoxy silane (B) acrylo silane (C) aldehyde silane (D) hydrophilic, sodium hydroxide treated glass slides.

3.2 Titanium Dioxide Loading

Negative controls were first fabricated by performing 5 hydrolysis reaction cycles on a substrate without assembled TMV templates. Figure 9 shows the AFM images of these samples made using both titanium (IV) butoxide and titanium (IV) isopropoxide precursors. Sharp color contrast indicates sudden height differences when the AFM tip comes in contact with particles on a higher level than the flat substrate surface. A strong affinity, specificity or preference for formation on the substrate surface would appear through AFM imaging as a more uniform color and height measurement. These images show that material formation does not have a strong specificity for the substrate, rather forming large, random aggregates of material.

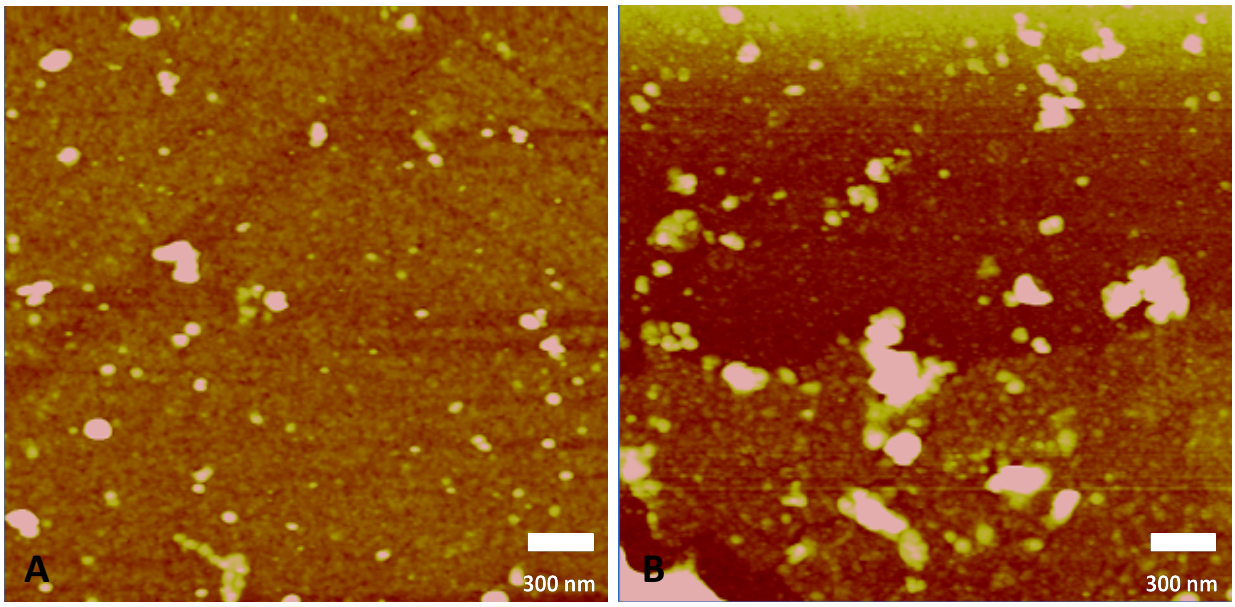

Figure 9: 3µm x 3 µm AFM images of aldehyde silane chips without TMV 1-cys assembly after 5 adsorption-hydrolysis cycles using precursors (A) TTIP and (B) TiBu.

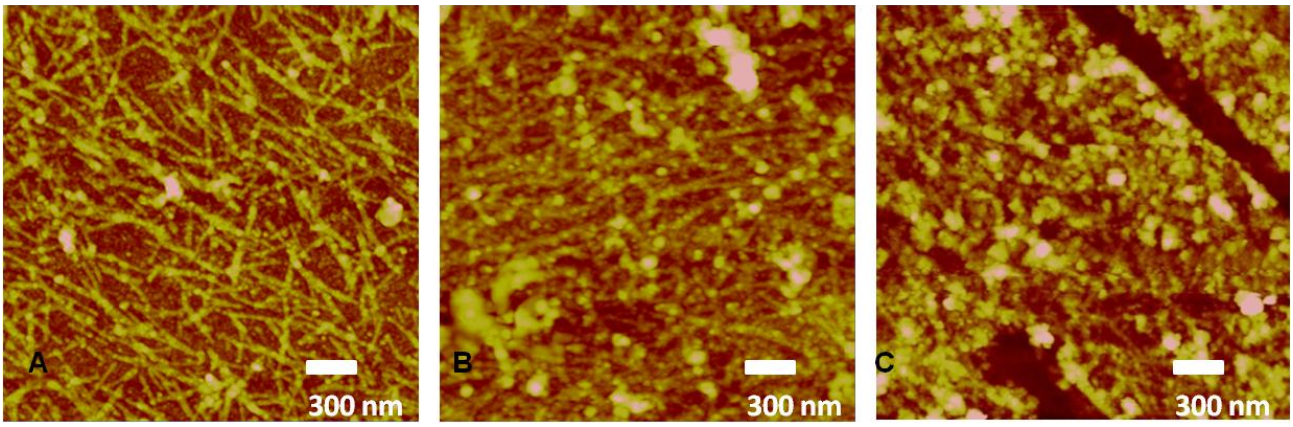

Figure **10** shows the AFM imaging of TMV assembled aldehyde silane chips after an increasing number of hydrolysis cycles. Larger particles and sharper contrast with increasing cycle number suggests an increasing amount of material forming on the template. Consistent background color also suggests preferential material formation on the TMV template over the substrate surface. The AFM imaging software confirms this, reporting heights of 12, 13 and 14nm for five, ten and fifteen cycles respectively, compared to a height of 9nm for the negative control sample containing TMV alone.

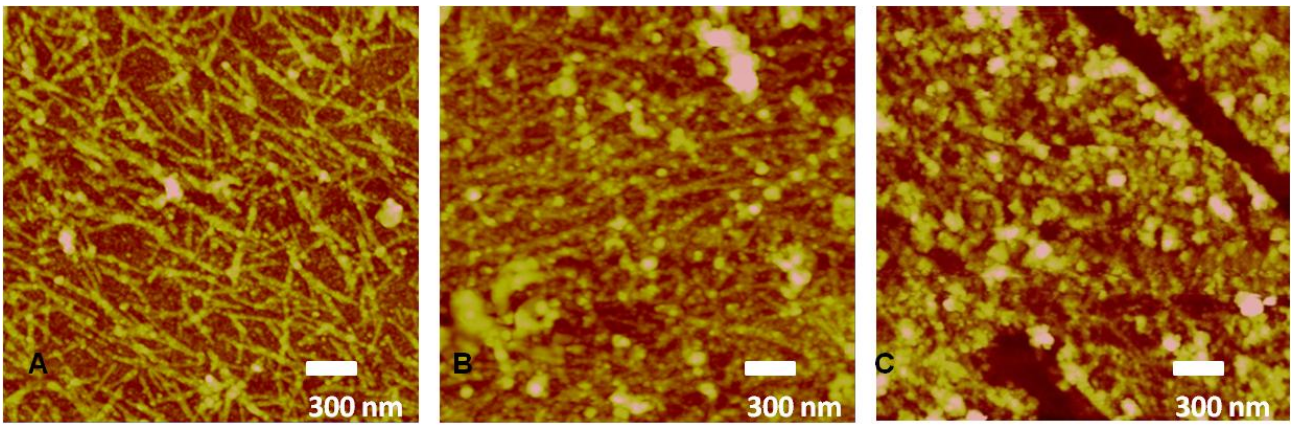

Figure 10: 3µm x 3 µm AFM images of TMV 1-cys catalyst chip after (a) five (b) ten (c) fifteen adsorption-hydrolysis cycles

In both the fabrication of control chips and catalyst chips, removal of the intermediate rinsing step caused the formation of a white film of solid material quickly and indiscriminately on all surfaces on which the precursor came in contact with water. When the solvent rinsing step is introduced however, both visual inspection and AFM imaging shows that titanium dioxide does not precipitate in solution and barely forms at all on the substrate surface but instead forms preferentially on TMV 1-cys rods bound to the chips surface. The difference between the control chips and TMV 1-cys assembled chips shows that the TMV 1-cys viral template is an effective means of controlling the otherwise the disordered and indiscriminant hydrolysis reaction of TTIP and TiBu to form titanium dioxide.

Both TTIP and TiBu are highly reactive with water precipitating solid films simply from exposure to humid air while in solution. Limited exposure to the air and thorough solvent rinsing and drying with inert gas between cycles prevented solid precipitation and ensured that only precursor molecules that had adsorbed onto the TMV 1-cys rods would be hydrolyzed.

Consistant TMV 1-cys coverage densities over several cycles demonstrates robustness of the viral template in maintaining its bond with the functionalized glass substrate despite thorough rinsing, strong reducers and mechanical manipulation such as glass cutting, dipping and physical contact with the substrate surface.

3.3 Platinum Loading

Platinum metal has been used previously to improve the catalytic efficiency of titanium dioxide[7]. To investigate the viability of using platinum metal in this context, TMV assembled aldehyde silane samples were loaded first with platinum metal and then exposed to 10 adsorption-hydrolysis cycles of titanium (IV) butoxide or titanium (IV) isopropoxide. These catalyst chips were fabricated to to compare with other platinum-titanium dioxide catalyst fabrication methods which involve calcining at very high temperatures. Figure 11 shows AFM images of sampels after the above procedures are performed in sequence. Uniform loading of small particles onto the TMV 1-cys rods is observed after the reduction of the platinum precursor with sodium borohydride. The same adsorption-hydrolysis procedure as described above was applied to the chip to form titanium dioxide on the subsequent layer.

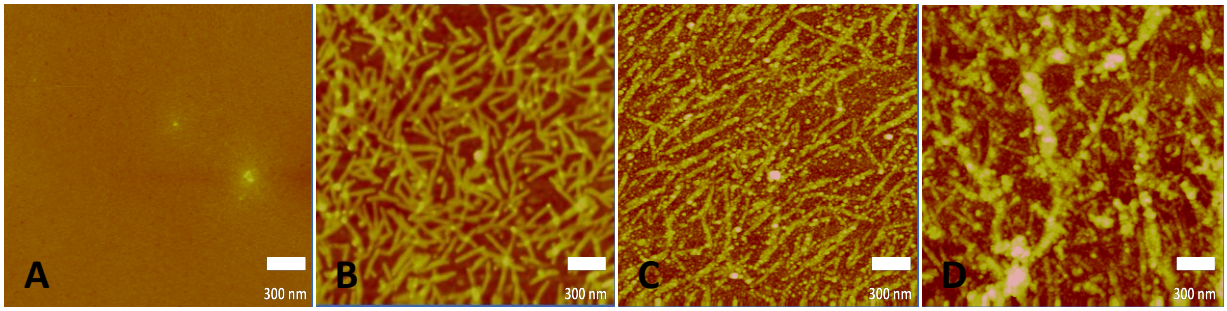

Figure 11: (A) Blank aldehyde silane chip. (B) TMV 1-cys assembled aldehyde silane chip (C) Pt loaded TMV 1-cys assembled aldehyde silane chip. (D) Titanium dioxide and Pt loaded TMV 1-cys assembled aldehyde silane chip

[7] Meng Ni, Michael K.H. Leung, Dennis Y.C. Leung, K. Sumathy, *A review and recent developments in photocatalytic water-splitting using TiO2 for hydrogen production* Renewable and Sustainable Energy Reviews Volume 11, 2007, Pages 401–425

3.4 Surface Characterization

While AFM imagining confirmed the changes in the morphology of the TMV and supported the idea of particle growth with increasing cycle number, the chemical identity of the material formed remains unconfirmed. To determine the surface chemistry of the surface material, ten representative samples were examined through XPS.

Table 1 describes the samples examined. Samples 1 and 2 were negative controls consisting only the functionalized glass and TMV assembled functionalized glass respectively. The XPS spectra produced by these samples were used for comparison.

List of Samples Analyzed by XPS				
Sample Label	**TMV solution concentration**	**$[Na_2PtCl_6]/[NaBH_4]$**	**Precursor**	**Number of Cycles**
1 (control)	-	-	-	-
2 (control)	0.1 mg/mL	-	-	-
3	0.1 mg/mL	-	Titanium butoxide	5
4	0.1 mg/mL	-	Titanium butoxide	10
5	0.1 mg/mL	-	Titanium butoxide	15
6	0.1 mg/mL	0.5mM/15mM	-	-
7	0.1 mg/mL	0.5mM/15mM	Titanium butoxide	10
8	0.1 mg/mL	0.5mM/15mM	Titanium Isopropoxide	10
9	0.1 mg/mL	0.5mM/15mM	Titanium butoxide	10
10	0.1 mg/mL	0.5mM/15mM	Titanium Isopropoxide	10

Table 1: List of Samples Analyzed by XPS

All peaks were identified by cross-reference through the NIST X-ray Photoelectron Spectroscopy Database which contains experimentally obtained binding energies of all elements and electron configurations as well as the compound analyzed to obtain the reading. The element and electron

configuration labels were added after referencing the database. An exhaustive listing of peaks for all the samples is given in the appendix. The left most peak in each spectrum is the OKLL reference and is not labeled in the spectra.

Survey spectra covering a wider range of binding energies (0-1000eV) were taken of all the samples to observe all changes in surface chemistry. The differences between the negative controls were noted first.

Figure 12 and Figure 13 show the XPS survey spectra of samples 1 and 2 respectively.

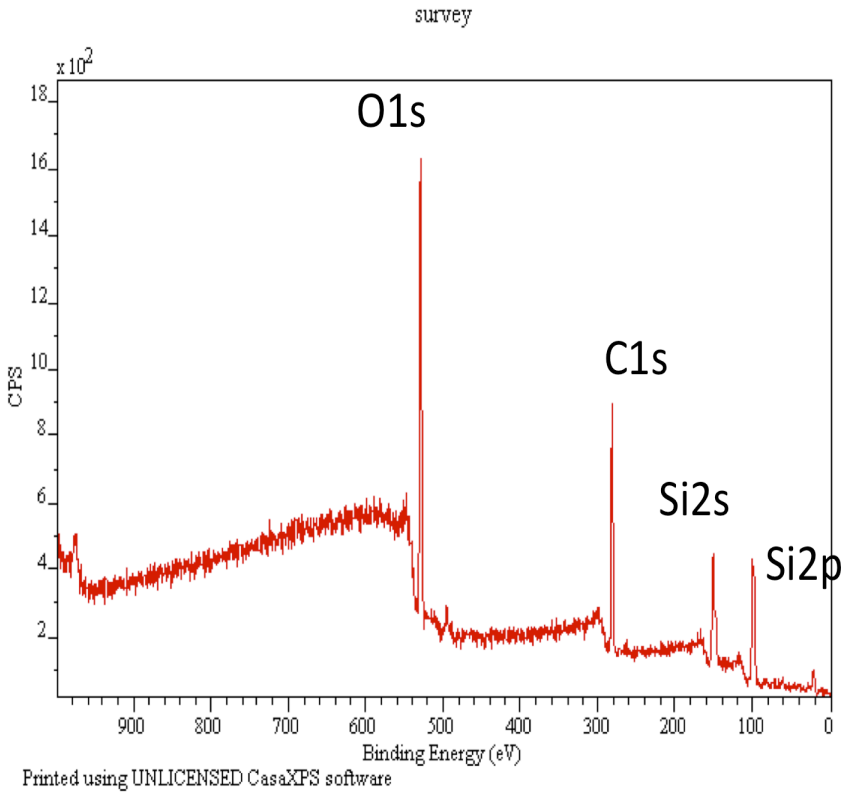

Figure 12: Survey spectra of control sample 1 consisting of aldehyde silane functionalized glass.

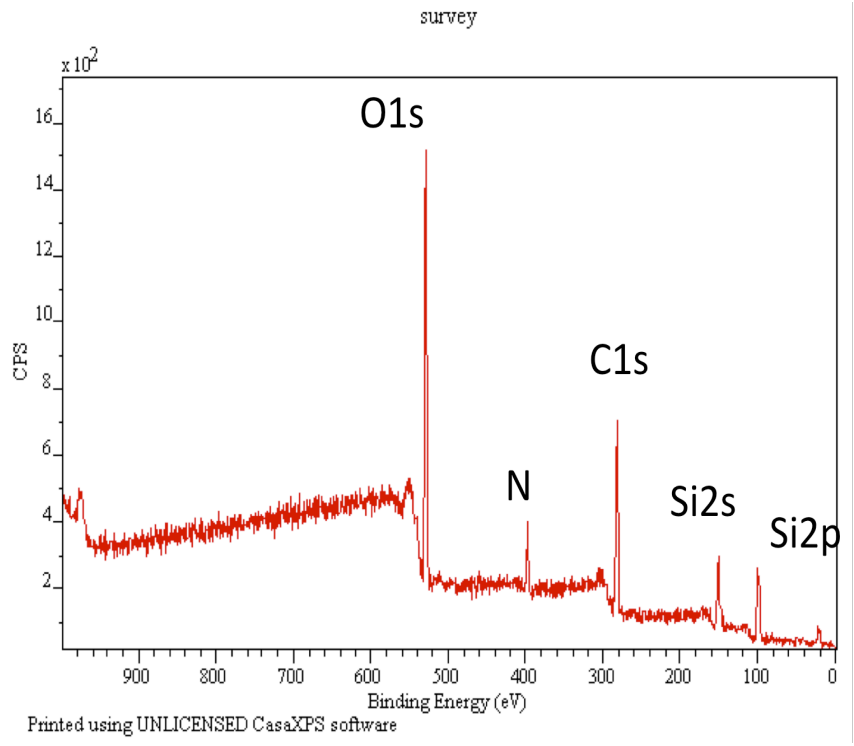

Figure 13: Survey spectra of control sample 2 consisting of TMV assembled aldehyde silane functionalized glass.

Sample 1 yielded peaks at 99.6, 150.3, 281.8 and 529.8eV corresponding to Si2p, Si2s, C1s and O1s configurations respectively. The two silicon peaks and oxygen peaks arise from the silicon dioxide (glass) chip. The relative areas of the oxygen and two silicon peaks give a ratio of 1:3 silicon to oxygen consistent with a silicon dioxide glass chip. The aldehyde functional groups on the surface of the chip are likely responsible for a slight excess in O1s counts. The carbon C1s peak at 281.8eV arises from both the aldehyde functional groups on the surface of the chip as well as any organic dust in the air that may have settled on the sample. This kind of contamination is common in surface analysis and the carbon peak in not used in any subsequent calculations.

The sample 2 spectrum (of TMV assembled glass) contains all the peaks yielded by sample 1 as well as a new nitrogen N1s peak at a binding energy of 398eV caused by the nitrogen containing proteins in TMV.

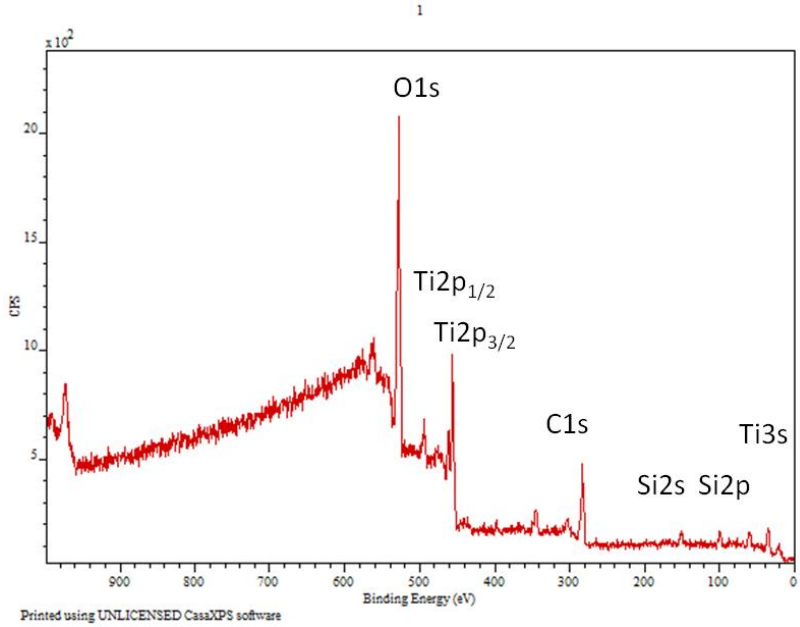

Figure 14: XPS spectrum of sample 3: TMV assembled aldehyde silane glass, 15 hydrolysis cycles.

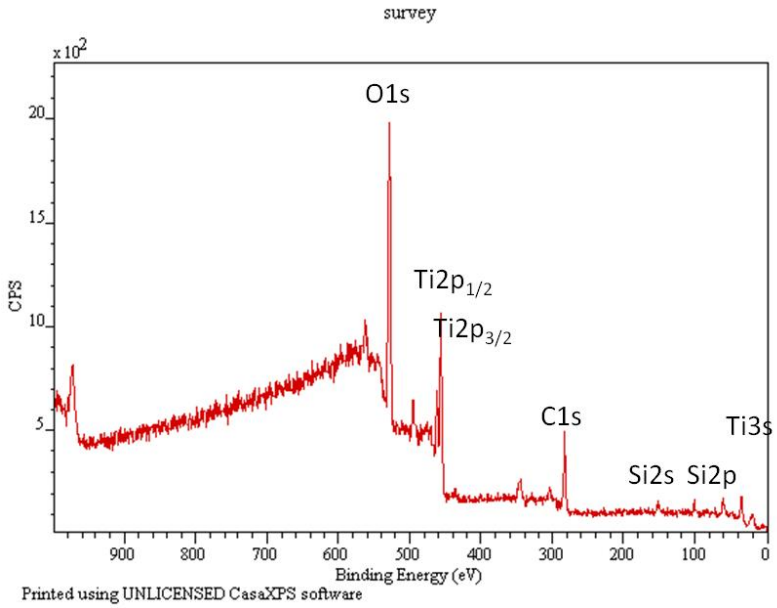

Figure 15: XPS spectrum of sample 4: TMV assembled aldehyde silane glass, 10 hydrolysis cycles

Figure 14 and Figure 15 show XPS spectra of samples 3 and 4 respectively of TMV assembled glass slides after five and ten cycles of hydrolysis respectively. These spectra show new peaks at 34.0, 456.7 and 462.3eV corresponding to the binding energies of Ti3p, $Ti2p_{1/2}$ and $Ti2p_{1/2}$ electrons respectively. While these electron configurations are present in a number of titanium containing compounds, given the well documented nature of the reactions performed, it is known that these titanium peaks are due to the presence of titanium dioxide and titanium trioxide (Ti_2O_3)[8].

In addition to the new titanium peaks, the N1s peak has diminished almost completely in these spectra, comprising less than 1% of the area of the significant peaks present. The disappearance of the nitrogen peak and the appearance of the titanium peaks shows that the surface of the sample was changed after the reaction procedures. The titanium containing material occluded the nitrogen containing layer described by the sample 2 spectrum so that only an insignificant amount of nitrogen was detectable by the XPS. Near complete coverage of the sample surface by the titanium containing compounds was achieved in both the five and ten cycle sample.

[8] Haimei Liu, Wensheng Yang, Ying Ma, Jiannian Yao, Extended visible light response of binary TiO2-Ti2O3 photocatalyst prepared by a photo-assisted sol-gel method, Applied Catalysis A: General, Volume 299, 17 January 2006, Pages 218-223, ISSN 0926-860X, DOI: 10.1016/j.apcata.2005.10.041.

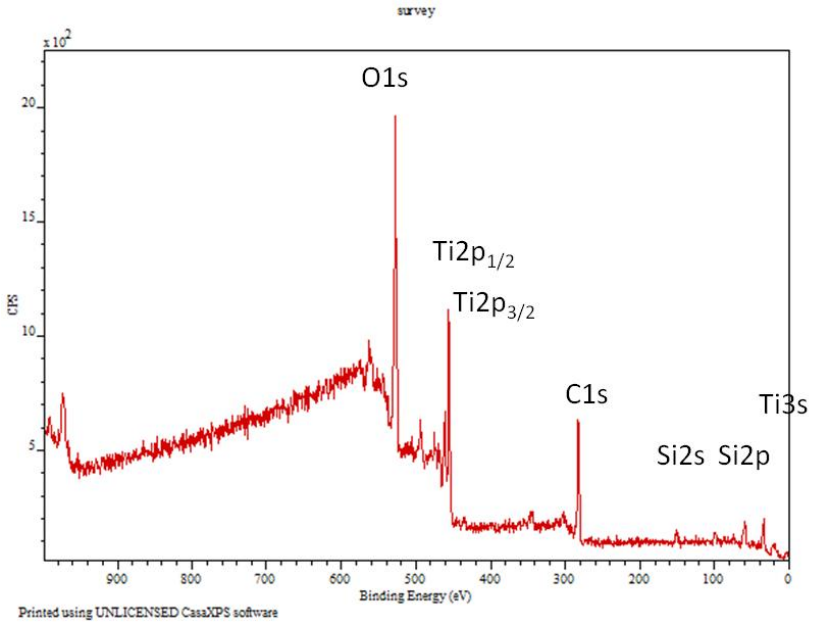

Figure 16: XPS spectrum of sample 5: TMV assembled aldehyde silane glass, 15 hydrolysis cycles

Surface Composition Comparison of Titanium Containing Samples		
Sample	**Cycles**	**Ti:O**
3	5	0.50
4	10	0.54
5	15	0.51

Table 2: Surface comparison of samples 3, 4 and 5 based on relative XPS peak area

Figure 16 shows the spectrum of the 15 cycle equivalent of samples 3 and 4. The relative amounts of titanium and oxygen was calculated and compared between the five ten and fifteen cycle sample using the areas of the peaks. The results of this calculation are shown in Table 2. The similarities between the three spectra and consistency of the surface chemistry show that the surface chemistry and relative amounts of the elements present on the surface of the sample does not change with increasing cycle

number. The same reaction occurred during each cycle producing a material at the surface that remains constant through at least 15 hydrolysis cycles.

The XPS data has shown that titanium containing compounds exist on the surface of the samples and in a ratio that is consistent with that of titanium dioxide. A single peak produced in the XPS spectra can consist of multiple component peaks that are used to identify the oxidation state of is corresponding element. To further support the presence of this material, a more detailed analysis of the $Ti2p_{1/2}$ and $Ti2p_{3/2}$ peaks was conducted by peak fitting using Casa XPS software. Figure 17, Figure 18 and Figure 19 show the peak fittings obtained for the $Ti2p_{1/2}$ and $Ti2p_{3/2}$ peaks in sample 3, 4 and 5. The best peak fittings for samples 3, 4 and 5 yeilded a residual standard deviation of 1.8, 2.3 and 2.2 from four component peaks compared to a fit of three component peaks which yeilded a standard deviation of 2.7, 3.0 and 2.9 while two peaks gave 9.3, 8.1 and 9.2. These four component peaks, two of which correspond to a +3 oxidaiton state while the other two correspond to a +4 oxidation state, sum closely to fit the original XPS spectrum. The left peak corresponds to the +4 state at a higher energy and the right peak corresponds to the +3 state at a lower energy. Because titanium dioxide contains titanium in a +4 oxidation state and titanium trioxide contains titanium in a +3 oxidation state, area analysis of the component peaks was conducted to determine the relative amounts of both species on the sample surface.

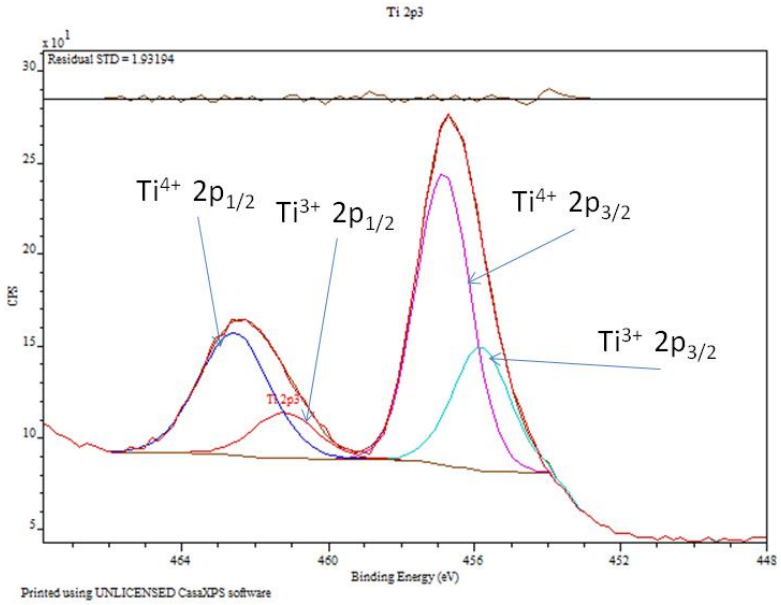

Figure 17: Peak fitting of XPS spectrum of sample 3

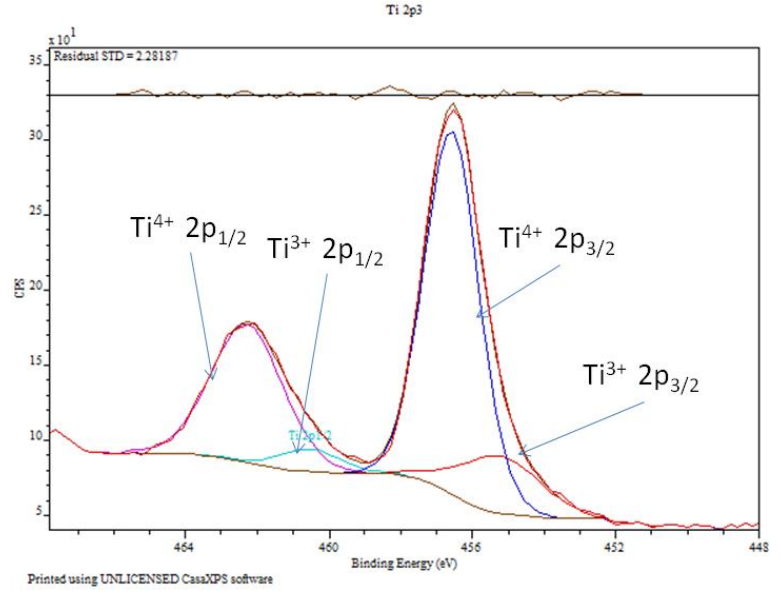

Figure 18: Peak fitting of XPS spectrum of sample 4

Similar area calculations to that comparing relative titanium and oxygen amounts were performed to determine the relative amounts of titanium dioxide and titanium trioxide. The ratio of oxygen to

titanium calculated previously as well as the first impressions of the peak fittings indicates that titanium dioxide is present in greater amounts than titanium trioxide. Area calculations summarized in Table 3 support this claim.

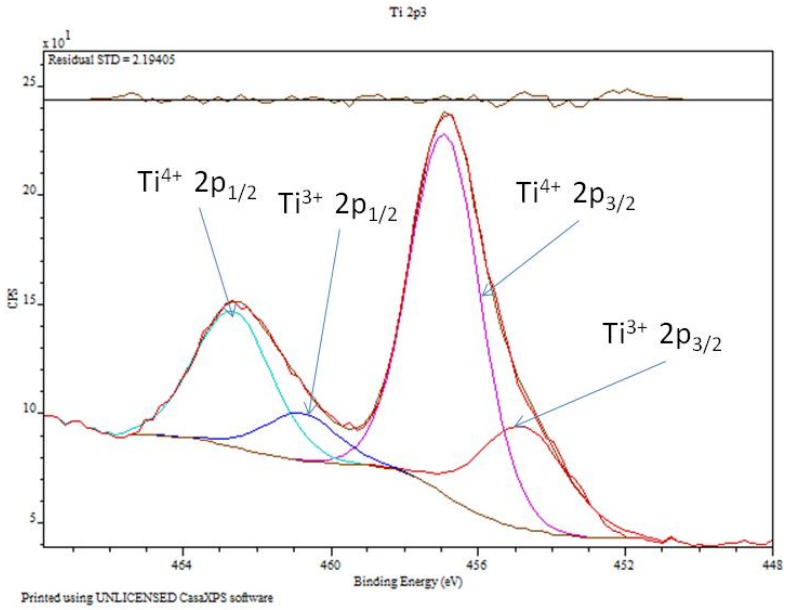

Figure 19: Peak fitting of XPS spectrum of sample 5

Oxidation State Comparison of Titanium Containing Samples		
Sample	**Cycles**	**% Ti^{4+}**
3	5	0.71
4	10	0.83
5	15	0.84

Table 3: Portion of surface titanium in the +4 oxidation state

To better assess the level of coverage of the titanium dioxide layer, a platinum base was first loaded onto the initial TMV-1cys layer through the reduction of a Na_2PtCl_6 platinum precursor with a sodium

borohydride reducing agent according to the procedure described above. The platinum formed on this layer is easily detected by XPS and its spectrum is shown in
Figure **20**. When the titanium dioxide layer is formed above the platinum, an incomplete coating would yield platinum peaks on the surface spectrum of the sample. Platinum was used in this experiment because it has previously been grown on TMV bio-templates[9] and has also been used to increase the activity of titanium dioxide in water splitting reactions.[10]

Sample 6 is a control that did not undergo the titanium dioxide precursor hydrolysis reactions and is used for comparison. The XPS spectrum of sample 6, shown in
Figure **20**, displays new peaks at 52.6, 71.3, 313.8, 330.7 and 518.5eV binding energies corresponding to $5p_{3/2}$, $4f_{7/2}$, $4d_{5/2}$, $4d_{3/2}$ and $4p_{3/2}$ platinum electron configurations respectively. Similarly to samples 3-5, sample 6 eliminates the nitrogen peak that arises from the exposed TMV rods on the surface of the sample, suggesting a complete coating of the viral template by platinum containing compounds. Platinum metal is indicated by the peaks at lower binding energies and the higher binding energy peaks can arise from higher oxidation state platinum oxides such as PtO_2 and $Pt(OH)_4$.

Samples 7-10 contain duplicates of samples fabricated with ten hydrolysis cycles of titanium (IV) isopropoxide and ten hydrolysis cycles of titanium (IV) butoxide. The XPS spectra of the corresponding samples are compared for consistency. Figure 21 and Figure 23 show the XPS spectra of samples 7 and 9 respectively fabricated with the titanium (IV) butoxide precursor. These spectra both contain the peaks observed in samples 3-5 and do not contain any of the five platinum peaks observed in the spectrum of control sample 6. A complete and uniform titanium dioxide coating of TMV and platinum has eliminated the representative peaks of the base layer in both samples. These spectra instead yield characteristic peaks of titanium dioxide at its representative binding energies

[9] Sang-Yup Lee, Jaewon Choi, Elizabeth Royston, David B. Janes, James N. Culver, Michael T. Harris, Deposition of Platinum Clusters on Surface-Modified Tobacco Mosaic Virus, Journal of Nanoscience and Nanotechnology Volume 6, April 2006, pages 974-981(8), doi:10.1166/jnn.2006.146

[10] G.R. Bamwenda, S. Tsubota, T. Nakamura and M. Haruta, Photoassisted hydrogen production from a waterethanol solution: a comparison of activities of Au-$TiO_2$and Pt-TiO_2, *J Photochem Photobiol A: Chem* **89** (1995), pp. 177–189.

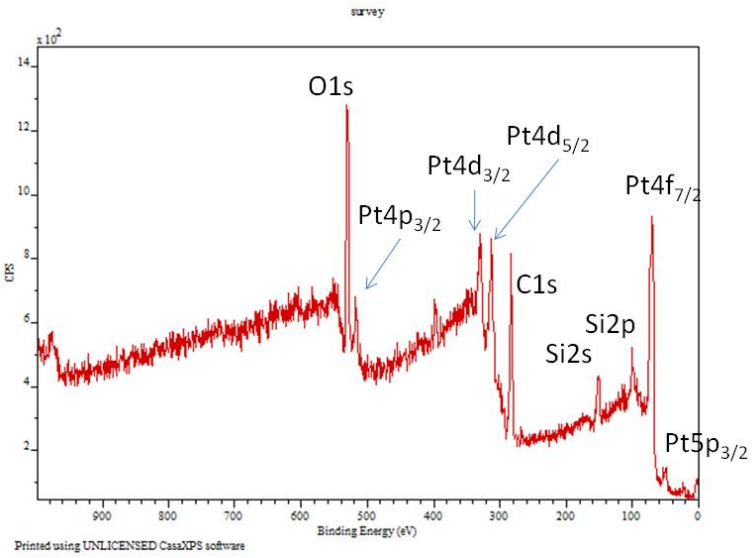

Figure 20: XPS spectrum of sample 6 consisting of TMV assembled aldehyde silane glass after platinum loading

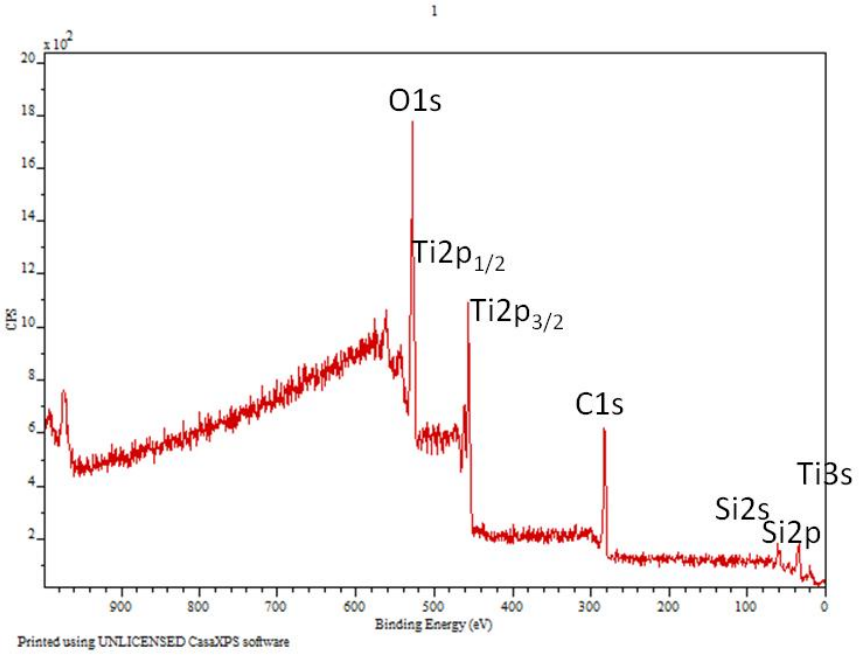

Figure 21: XPS spectrum of sample 7 consisting of TMV assembled aldehyde silane glass after platinum loading and 10 cycles of titanium (IV) butoxide hydrolysis.

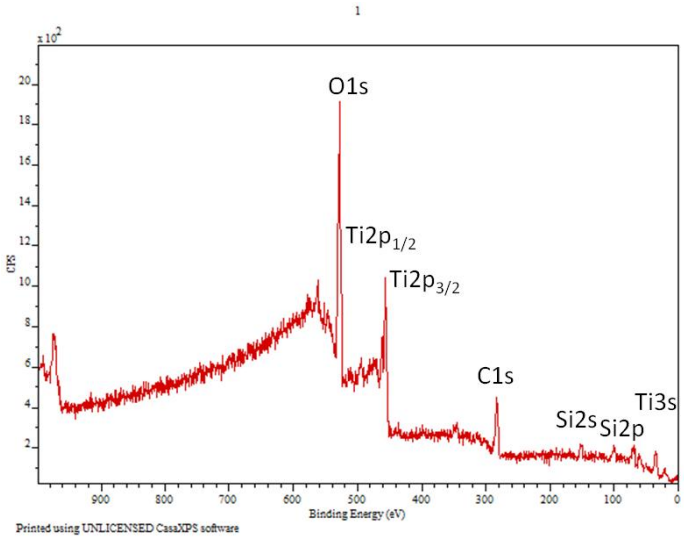

Figure 22: XPS spectrum of sample 8 consisting of TMV assembled aldehyde silane glass after platinum loading and 10 cycles of titanium (IV) isopropoxide hydrolysis.

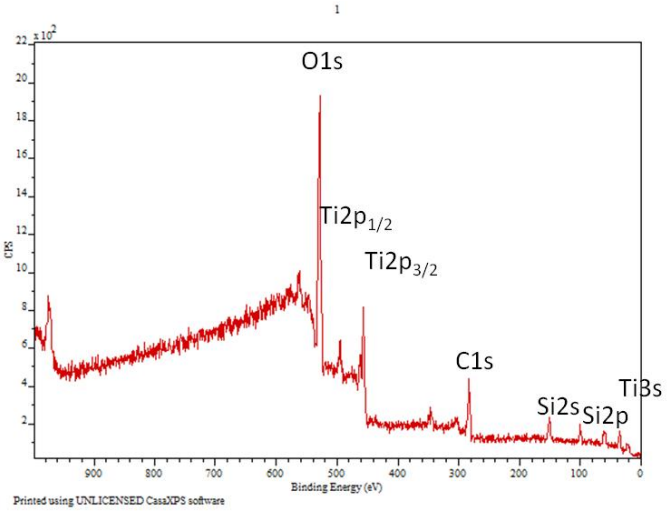

Figure 23: XPS spectrum of sample 9 consisting of TMV assembled aldehyde silane glass after platinum loading and 10 cycles of titanium (IV) butoxide hydrolysis.

Figure 22 and **Figure 24** show the XPS survey spectra of samples 8 and 10 respectively fabricated using the titanium (IV) isopropoxide precursor. Similarly to samples 7 and 9, these samples do not exhibit any

platinum peaks as observed in control samples 6. However, the representative peaks of titanium dioxide at its binding energies are displayed indicating thorough coverage of the base layer

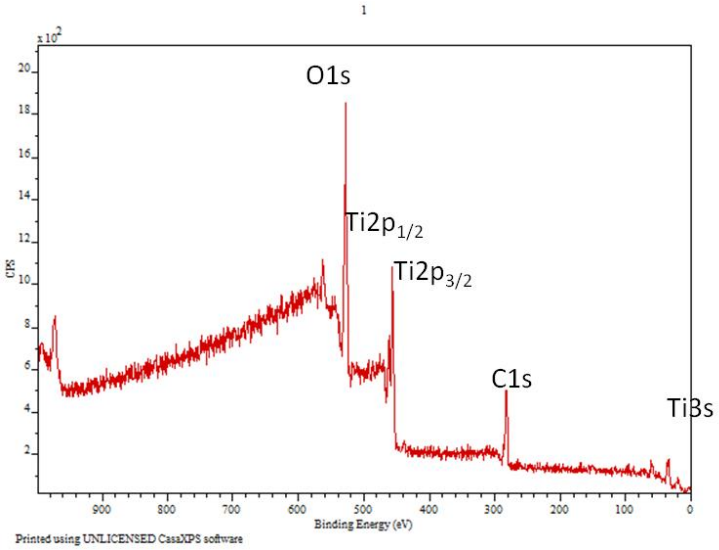

Figure 24: XPS spectrum of sample 10 consisting of TMV assembled aldehyde silane glass after platinum loading and 10 cycles of titanium (IV) isopropoxide hydrolysis

Most samples analyzed through XPS contained silicon peaks at 100 and 150eV binding energies consistent with the 2s and 2p electron configurations of silicon in glass. Figure 21, however, does not display silicon peaks as in the other samples suggesting complete coverage of the entire substrate surface. That these peaks were often not occluded after any of the procedures performed as were the nitrogen peaks indicative of TMV, shows preferential material formation on the biotemplate and not the glass substrate. This observation is also consistent with observations of AFM imaging in which material did not form on substrates alone. Analysis through XPS confirmed that the precursor hydrolysis reactions successfully formed titanium dioxide, that the titanium dioxide layer formed a complete coating over both titanium and TMV layers after 10 cycles and that both precursors are capable of producing complete and preferential coating of TMV templates.

3.5 Activity Characterization

Negative control experiments were conducted first according to the procedure outlined above. These experiments did not utilize the fabricated chips but simply measured the amount of dissolved oxygen in water over time while exposed to the same conditions. Two experiments under the same negative control conditions were executed and the results of the change in oxygen over time are shown in Figure 26. Because the temperature of the UV chamber rose over time during the experiment according to the heating curve measured during the experiment and shown in Figure 25, the amount of dissolved oxygen was expected to decrease. Figure 26 confirms this as the dissolved oxygen levels in the first and second negative control runs decreased by 0.33 and 0.20 mg/L over 37.0 and 34.7°C temperature increases respectively. The pressure within the flask of the negative control runs remained constant throughout the experiment indicating a tight seal. Because of the consistency between the behavior of the two negative controls performed on different days with different humidity conditions and with different starting dissolved oxygen levels, it is assumed that present relative humidity conditions and the starting amount of dissolved oxygen at these low levels (0.7 and 1.52 mg/L) do not significantly affect the change of dissolved oxygen amounts in this system.

Oxygen Solubility	
Temperature (°C)	**Oxygen Solubility (mg/L)**
0	14.6
5	12.8
10	11.3
15	10.1
20	9.1
25	8.3
30	7.6
35	7
40	6.5
45	6
50	5.6

Table 4: Oxygen solubility over a range of temperatures[11]

[11] Oxygen Solubility in Fresh and Sea Water. Solubility of oxygen in equilibration with air in fresh and sea (salt) water - pressures ranging 1 - 4 bar abs. The Engineering ToolBox. (http://www.engineeringtoolbox.com/oxygen-solubility-water-d_841.html

The experiments performed all occur at dissolved oxygen levels significantly below the saturation levels of oxygen in water listed at various temperatures in Table 4.

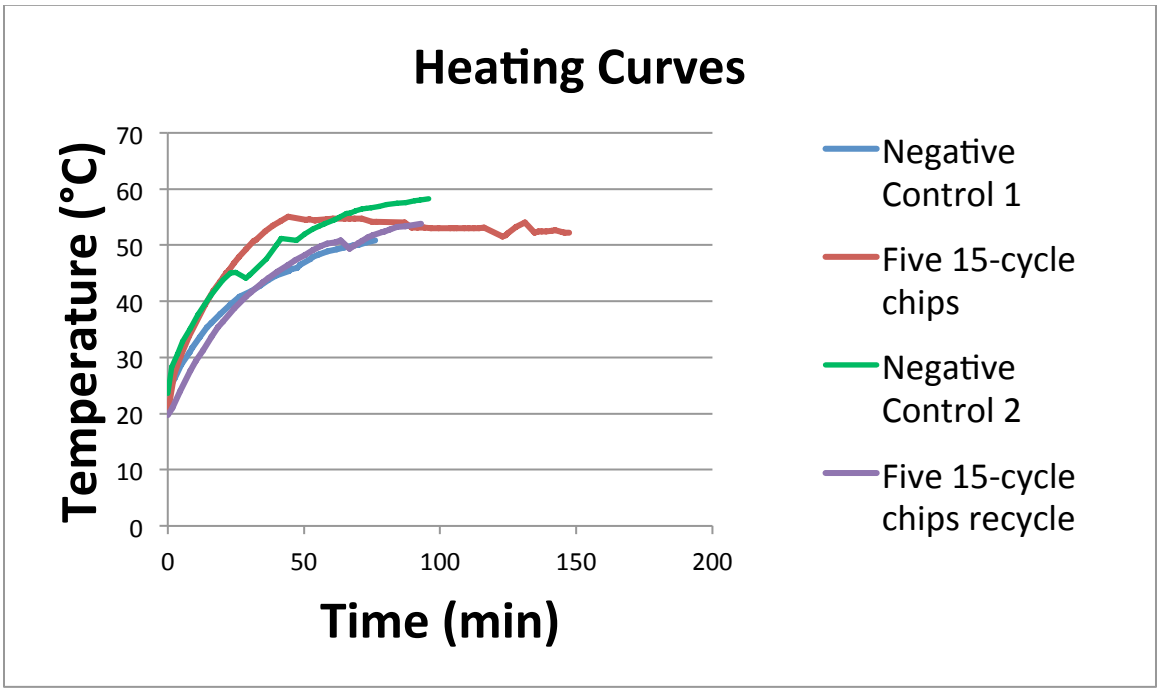

Figure 25: Heating curves for all experiments

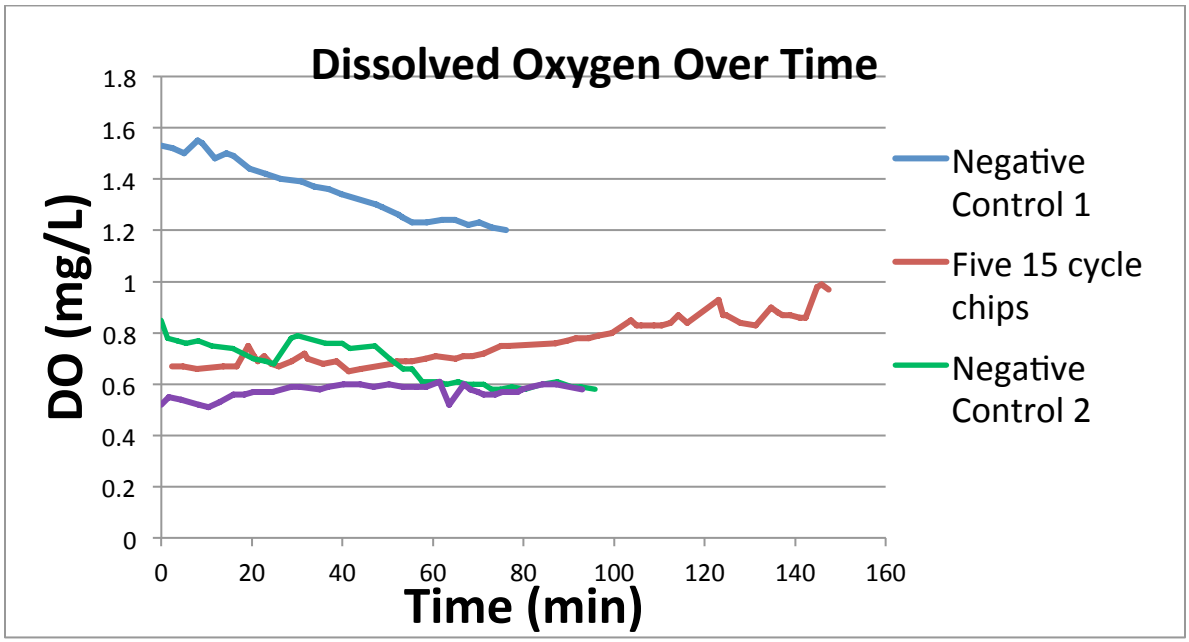

Figure 26: Dissolved oxygen measurements two negative control experiments, fabricated chips experiments and recycle experiment

Five chips fabricated using fifteen cycles of hydrolysis of titanium (IV) butoxide were then tested. Two runs performed using the same chips were executed on different occasions. The second experiment using the same chips was used as a recycle test for comparison to the unused chips. The change in dissolved oxygen for the first and recycle experiments are shown in Figure 26. The first run shows an overall increase in dissolved oxygen over the course of the 147min experiment despite a 32°C increase in temperature compared to the negative control experiments which resulted in an overall decrease. The heating curves of these experiments are similar to those of the negative control experiments and show that the differences between the change in dissolved oxygen levels is not due to differences in temperature. A consistent increase in the pressure measurement inside the flask is another significant difference between these experiments and the negative controls. While the negative control experiments maintained a constant pressure over the course of the run, the pressure of the first run containing the fabricated chips increased from 759.7 to 761.9mmHg . Because of tight sealing procedures and because the pressure within the flask exceeded that of the atmospheric pressure that day, a sealing leak could not have cause the pressure changes.

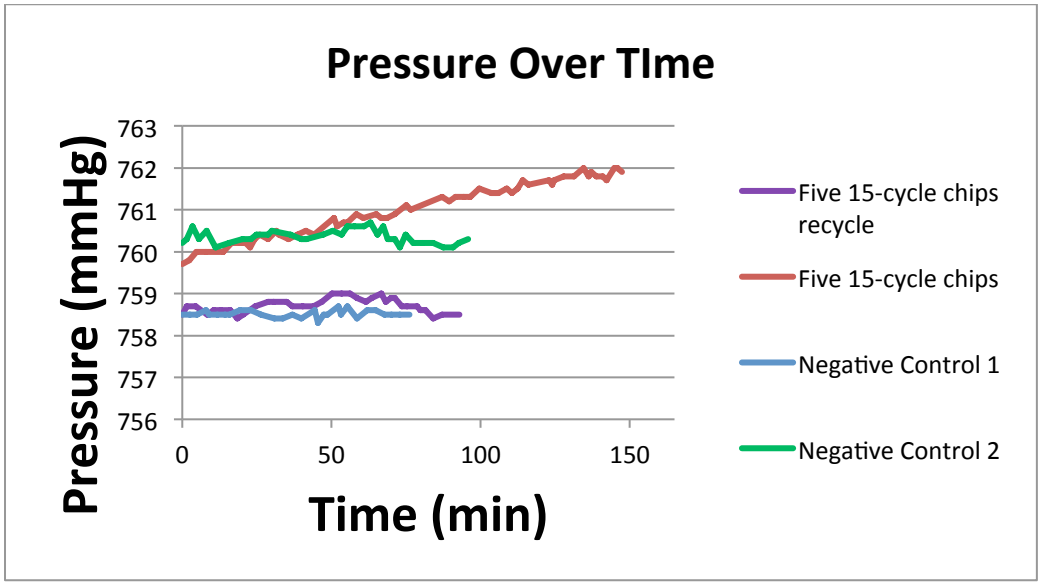

Figure 27: Pressure measurements over time for all experiments

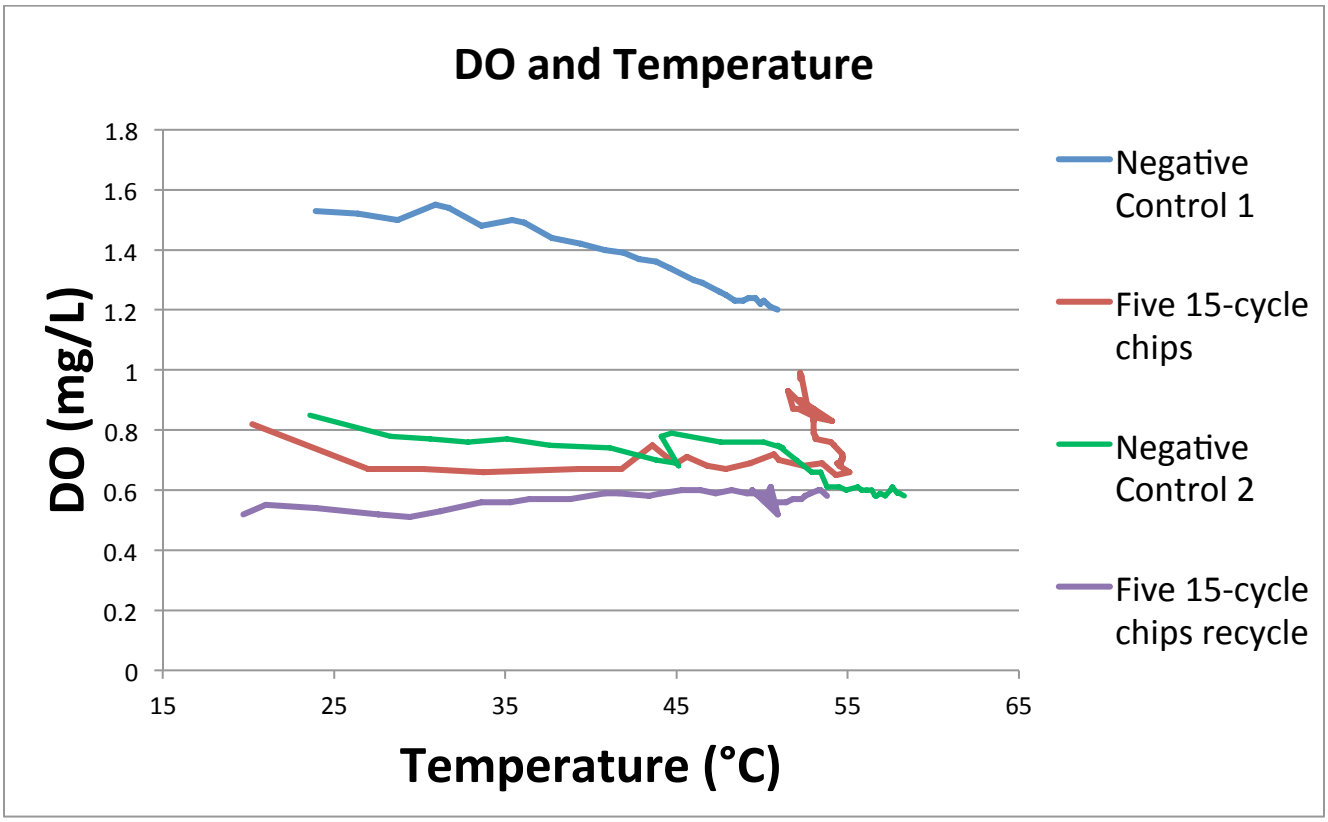

Figure 28: Dissolved oxygen measurements versus temperature for all experiments

A plot of the dissolved oxygen levels versus temperature provides useful information for the comparison of experiments. Figure 28 shows that for the negative control experiments, the dissolved oxygen predictably decreases as the temperature in the UV chamber rises. The first experiment involving the fabricated chips however maintains a relatively constant dissolved oxygen reading of about 0.66mg/L over the temperature range of 20.2 to 53.4°C. At 61min when the temperature remains relatively constant for the following 87min, the dissolved oxygen levels rise. This experiment has shown that the initial presence of the chips fabricated in earlier stages increases the amount of dissolved oxygen in water. It has also been shown that temperature changes are not the cause of the differences in the behavior when compared to the negative controls and that an increase in pressure accompanies the increase in dissolved oxygen.

The second experiment used the same chips as in the first. This resulted in behavior that was somewhat more like that of the negative controls. The pressure in the flask during this experiment remained relatively constant and did not change from 758.3mmHg at the start of the experiment to the end 93 min later. Dissolved oxygen levels increased only 0.06mg/L over the course of the experiment compared to the 0.3mg/L increase during the first experiment. The recycle experiment behaved like the negative controls in that the pressure remained constant throughout the experiment but also behaved like the previous experiment in that an overall increase in dissolved oxygen resulted. It is possible that these results are due to a spent catalyst. After reaction occurring in the first 147min experiment, drying and storing for several days, it is possible the catalytic material degraded, changed its mineral form, or its surface was harmed.

An increase of 0.15mg/L dissolved oxygen in the first fabricated chip experiment corresponds to a 0.12mmol production of O_2 over the course of the 147min experiment. Because the temperature in reaction vessel was increasing throughout the experiment, the observed dissolved oxygen increase is an underestimate of the actual amount of oxygen produced. If at least 0.15mg/L of oxygen is produced, then it is expected that twice the amount of hydrogen is produced according to Equation 4. This means that at least 0.24mg/L of hydrogen must have been produced.

The near liner increase in dissolved oxygen that occurs after 40min suggests that the maximum rate of the reaction has been achieved. Given the small amount of titanium dioxide present on the chip surface (on the order of 10^{-6}g) relative to the 25mL of deionized water present, it is assumed that the concentration of water remains constant over the course of the experiment despite the reaction taking place. If the rate of the reaction can be expressed according to Equation 5, and the concentration of water in the flask is constant and equal to the concentration of pure water, then the maximum rate of

the reaction may be inferred from experimental data and the reaction constant, k may be calculated after a reaction order is assumed.

$$\frac{d[O_2]}{dt} = k[H_2O]^n$$

Equation 5: Assumed rate law.

According to the above assumptions, the maximum rate of reaction is calculated to be 1.1µmol/min. The calculation of the rate constant for the reaction would depend on the order of the reaction. Because the concentration of water was assumed constant throughout the experiment, the reaction order cannot be inferred. At a constant water concentration, similar behavior would be expected for a reaction described by Equation 5 where n is any value. To determine more about the kinetics of the reaction, a smaller reaction volume may be used so that an observable decrease in water concentration causes the reaction to be limited by the diffusion of water to the reaction surface instead of the reaction kinetics.

4. Conclusions

AFM Imaging of various TMV assembled substrates showed that aldehyde functionalized glass slides are capable of achieving high, uniform surface coverage densities comparable to that of more expensive gold substrates. Tunable surface density is also possible through this substrate and offers control over the number of templates assembled on the surface and therefore the number of sites for possible particle growth. Further imaging through AFM showed that the hydrolysis reactions of titanium (IV) butoxide and titanium (IV) isopropoxide precursors preferentially forms material on TMV templates that increases in size with increasing cycle numbers providing control over the amount of material formed. XPS analysis showed that the surface material created from the precursors consists mainly of titanium dioxide, some titanium trioxide and thoroughly coats the TMV templates. Platinum loading of the TMV prior to the execution of precursor hydrolysis is also possible through the method described in this

experiment. Activity testing through water splitting reactions showed that the presence of the chips fabricated using this method is capable of increasing the dissolved oxygen levels in deionized water when exposed to ultraviolet light. Fabrication of nanoscale catalysts through methods described here is a necessary step towards the development of more efficient material.

5. Appendix

Sample 1: AlS chip			
Peak #	**Binding Energy (eV)**	**Area**	**Identity**
1	529.9208	995.6	O1s
2	281.3592	2059.9	C1s
3	150.301	1153.7	Si2s
4	99.574	971.2	Si2p

Table 5: Table of peaks yielded by Sample 1

Sample 2			
Peak #	**Binding Energy (eV)**	**Area**	**Identity**
1	529.81	5059.4	O1s
2	396.418	603.4	N1s
3	281.841	2010.4	C1s
4	150.301	667.7	Si2s
5	99.574	609.9	Si2p

Table 6: Table of peaks yielded by Sample 2

Sample 3: AlS-TMV-TIPP5			
Peak #	**Binding Energy (eV)**	**Area**	**Identity**
1	528.1386	6846.823	O1s
2	462.2574	218.17	Ti2p1/2
3	456.729	3188.657	Ti2p3/2
4	283.693	1532.553	C1s
5	149	150.3	Si2s
6	100.4498	214.993	Si2p
7	60.387	217.6	Ti3s

Table 7: Table of peaks yielded by Sample 3

Sample 4			
Peak #	**Binding Energy (eV)**	**Area**	**Identity**
1	532.69	6469.3	O1s
2	462.059	752.3	Tip1/2
3	456.515	2348.7	Ti2p3/2
4	282.8	1271.5	C1s
5	151.5	240.2	Si2s
6	100.4	134.3	Si2p
7	60.387	233.1	Ti3s

Table 8: Table of peaks yielded by Sample 4

Sample 5: AlS -TMV -TiBu15			
Peak #	**Binding Energy (eV)**	**Area**	**Identity**
1	536.455	1333.1	Os1
2	469.265	179.8	Ti2p1/2
3	464.904	503.9	Ti2p3/2
4	290.355	944.2	C1s
5	157.8	102.7	Si2s
6	107.3	96.3	Si2p
7	68.1	154.1	Ti3s

Table 9: Table of peaks yielded by Sample 5

Sample 6			
Peak #	**Binding Energy (eV)**	**Area**	**Identity**
1	529.81	3171	O1s
2	518.538	840.4	Pt4p3/2
3	330.662	1603.2	Pt4d3/2
4	313.753	2179.6	Pt4d5/2
5	283.693	2200.4	C1s
6	152.18	545.8	Si2s
7	101.453	311.3	Si2p
8	71.326	3938.8	Pt4f7/2
9	52.605	225.4	Pt5p3/2

Table 10: Table of peaks yielded by Sample 6

Sample 7			
Peak #	**Binding Energy (eV)**	**Area**	**Identity**
1	528.139	1183.6	Os1
2	462.455	198.6	Ti2p1/2
3	456.713	588.2	Ti2p3/2
4	282.4	470.7	C1s
5	60.9695	311.3	Ti 3s

Table 11: Table of peaks yielded by Sample 7

Sample 8			
Peak #	**Binding Energy (eV)**	**Area**	**Identity**
1	529.921	6820.7	Os1
2	463.842	543.8	Ti2p1/2
3	456.3	2398.9	Ti2p3/2
4	282.8	1360.4	C1s

5	151.9	203.0	Si2s
6	100.4	239.9	Si2p
7	60.9	271.5	Ti3s

Table 12: Table of peaks yielded by Sample 8

Sample 9			
Peak #	**Binding Energy (eV)**	**Area**	**Identity**
1	529.525	6651.2	Os1
2	462.842	391.1	Ti2p1/2
3	457.117	1824.0	Ti2p-Ti2p3/2
4	283.083	1078.3	C1s
5	151.153	321.1	Si2s
6	100.661	259.8	Si2p
7	59.212	298.1	Ti3s

Table 13: Table of peaks yielded by Sample 9

Sample 10			
Peak #	**Binding Energy (eV)**	**Area**	**Identity**
1	528.535	5796.2	Os1
2	463.248	760.0	Ti2p1/2
3	457.191	2236.1	Ti2p-Ti2p3/2
4	283.387	1471.5	C1s
5	60.623	173.4	Ti3s

Table 14: Table of peaks yielded by Sample 10

6. Works Cited

Meng Ni, Michael K.H. Leung, Dennis Y.C. Leung, K. Sumathy, A review and recent developments in photocatalytic water-splitting using TiO2 for hydrogen production, Renewable and Sustainable Energy Reviews, Volume 11, Issue 3, April 2007, Pages 401-425

Sang-Yup Lee, Jaewon Choi, Elizabeth Royston, David B. Janes, James N. Culver, Michael T. Harris, Deposition of Platinum Clusters on Surface-Modified Tobacco Mosaic Virus, Journal of Nanoscience and Nanotechnology Volume 6, April 2006, pages 974-981(8).

G.R. Bamwenda, S. Tsubota, T. Nakamura and M. Haruta, Photoassisted hydrogen production from a waterethanol solution: a comparison of activities of Au-$TiO_2$and Pt-TiO_2, *J Photochem Photobiol A: Chem* 89 (1995), pp. 177–189.

Haimei Liu, Wensheng Yang, Ying Ma, Jiannian Yao, Extended visible light response of binary TiO2-Ti2O3 photocatalyst prepared by a photo-assisted sol-gel method, Applied Catalysis A: General, Volume 299, 17 January 2006, Pages 218-223.

A Klug. The tobacco mosaic virus particle: structure and assembly. Philosophical Transactions Royal Society London B Biological Sciences. 1999 March 29; 354(1383): 531–535

Takayuki Hirai, Hiroshi Sato, Isao Komasawa. Mechanism of formation of titanium dioxide ultrafine particles in reverse micelles by hydrolysis of titanium tetrabutoxide. T*Industrial & Engineering Chemistry Research* 1993 *32* (12), 3014-3019

C. Su, B.-Y. Hong, C.-M. Tseng, Sol-gel preparation and photocatalysis of titanium dioxide, Catalysis Today, Volume 96, Issue 3, Materials Design in Catalysis - Symposium C of ICMAT 2003, 5 October 2004, Pages 119-126.

Charles D. Wagner, Alexander V. Naumkin,Anna Kraut-Vass, Juanita W. Allison, Cedric J. Powell, and John R. Rumble, Jr. NIST X-ray Photoelectron Spectroscopy Database. Last updated: August 27, 2007 (Created: June 06, 2000) (http://srdata.nist.gov/xps/)

Oxygen Solubility in Fresh and Sea Water. Solubility of oxygen in equilibration with air in fresh and sea (salt) water - pressures ranging 1 - 4 bar abs. The Engineering ToolBox. (http://www.engineeringtoolbox.com/oxygen-solubility-water-d_841.html)

Junwang Tang, James R. Durrant, David R. Klug. Mechanism of Photocatalytic Water Splitting in TiO2. Reaction of Water with Photoholes, Importance of Charge Carrier Dynamics, and Evidence for Four-Hole Chemistry. *Journal of the American Chemical Society* 2008 *130* (42), 13885-13891